

Basic Study on Detection of Outer Boundary of Arterial Wall Using Its Longitudinal Motion

Takanori NUMATA, Hideyuki HASEGAWA, and Hiroshi KANAI*

Graduate School of Engineering, Tohoku University, Sendai 980-8579, Japan

(Received November 24, 2006; revised March 15, 2007; accepted March 22, 2007; published online July 26, 2007)

The longitudinal motion of the arterial wall can be observed in a B-mode image obtained by recent ultrasonic diagnostic equipment. In this study, the longitudinal displacement was quantitatively estimated by the block matching of RF echoes using cross correlation. However, the estimated longitudinal displacement is discrete depending on the spacing between two ultrasound beams of about 0.1 mm. Such an accuracy is not sufficient for tracking the region of interest (ROI) in the arterial wall. Therefore, the spacing of 0.1 mm is reduced using the interpolation of measured RF echoes to improve the tracking of the ROI in the displacement estimation. In this study, the optimum parameter in the interpolation was investigated. The spatial distribution of longitudinal displacements along the arterial radial direction was estimated using the optimum parameter. There were significant differences between the longitudinal displacements in the arterial wall and those in the region considered to be tissue outside the arterial wall. These results show the possibility of using this method to identify the outer boundary of the adventitia, which has not been achieved by conventional ultrasonic imaging.

[DOI: 10.1143/JJAP.46.4900]

KEYWORDS: longitudinal displacement, complex interpolation, block matching, correlation function, adventitia position

1. Introduction

Diagnosis of arteriosclerosis is important because it poses a serious risk of cardiovascular events. We developed a noninvasive method for measuring the elasticity of the arterial wall.^{1–7)} In this method, the boundaries of the arterial wall are assigned by manual inspection of a B-mode image. Therefore, a method of identifying the boundaries is required for the objective and reproducible estimation of the elasticity.

The carotid artery exhibits the expansion and contraction (radial movement) due to the change in blood pressure during one cardiac cycle. At the same time, the carotid artery moves in its longitudinal direction (longitudinal movement). Recently, there have been some studies on the measurement of the arterial longitudinal displacement.^{8–12)} In these studies, the displacement is estimated by the block matching^{8–14)} of received echoes in two frames using the cross-correlation function. The longitudinal displacement of the arterial wall is less than 1 mm during one cardiac cycle.¹¹⁾ Generally, the measurement in the carotid artery is carried out using a 10 MHz probe. The correlation function, which is a function of the longitudinal displacement, is discrete depending on the spacing between two ultrasonic beams of about 0.1 mm in the 10 MHz probe case. Therefore, the longitudinal displacement cannot be measured with an accuracy of less than 0.1 mm. Such an accuracy is not sufficient for tracking the region of interest (ROI) in the arterial wall.

In this study, the spacing of 0.1 mm is reduced by the interpolation of measured RF echoes to improve the tracking of the ROI in the displacement estimation. The purpose of this study is to determine the optimum number of interpolated lines. This parameter was determined by evaluating the variation in correlation coefficient due to the inherent noise of the measurement system. Using the determined number of interpolated lines, the longitudinal displacement and longitudinal stretch of the carotid artery were estimated. In

addition, the spatial distribution of longitudinal displacements of the carotid arterial wall along its radial direction was obtained, and the outer boundary of the arterial wall was estimated using the displacement distribution.

2. Methods

2.1 Complex linear interpolation of RF echoes

The ultrasound information was provided by an Aloka SSD-6500 ultrasonic system. Using an ultrasonic probe of 10 MHz frequency, an ultrasound beam scans positions along the carotid artery in its longitudinal direction with intervals of 0.1 mm. At each position, RF echoes are acquired at a sampling frequency of 40 MHz. A B-mode image can be constructed with a two-dimensional (radial-longitudinal) data set obtained by one scan, which is called a frame. The RF signal at beam position b and depth d in the n -th frame is denoted by $rf_n(d, b)$.

To reduce the spacing of two beams, K lines are interpolated between the original RF lines. Complex linear interpolation was used in this study. In the case of the interpolation of a real function, the interpolated waveform is distorted by the phase difference of echoes along two different beams. Therefore, in this study, the complex linear interpolation was applied to the quadrature demodulated complex signal, $z_n(d, b)$, of RF echo, $rf_n(d, b)$, as follows:

$$\left| z'_n \left(d, b + \frac{k}{K+1} \right) \right| = \frac{(K+1-k)|z_n(d, b)| + k|z_n(d, b+1)|}{K+1}, \quad (2.1)$$

$$\arg \left[z'_n \left(d, b + \frac{k}{K+1} \right) \right] = \frac{(K+1-k)\arg[z_n(d, b)] + k\arg[z_n(d, b+1)]}{K+1}, \quad (2.2)$$

$$(k = 0, 1, 2, \dots, K),$$

where $z'_n(d, b + k/(K+1))$ is the interpolated complex signal. Each interval of two beams is given by $\Delta w(K) = 0.1/(K+1)$ mm when K lines are interpolated between the original RF lines.

*E-mail address: hkanai@ecei.tohoku.ac.jp

2.2 Block matching using cross-correlation function

The radial and longitudinal displacements, $\widehat{x}_r(n)$ and $\widehat{x}_l(n)$, at the n -th frame are estimated using the correlation function between two frames including the interpolated complex signals.

First, the region of interest (ROI) is assigned in the initial frame. The center of the ROI at a time $t = n\Delta T$ (n -th frame) is defined as $d = d_n$ and $b = b_n$. Then, the complex correlation coefficient, $\gamma(n; \Delta m, \Delta l)$, between the n -th frame at a time $t = n\Delta T$ and the $(n + \Delta N)$ -th frame at a time $t = (n + \Delta N)\Delta T$ is calculated as follows:

$$\begin{aligned} \gamma(n; \Delta m, \Delta l) &= \frac{1}{(M+1)(L+1)\sigma\sigma'} \\ &\times \sum_{m=-M/2}^{M/2} \sum_{l=-L/2}^{L/2} Z_{m,l} Z_{m+\Delta m, l+\Delta l}^* \end{aligned} \quad (2.3)$$

$$Z_{m,l} = z'_n(d + mD, b + l\Delta w(K)), \quad (2.4)$$

$$Z'_{m,l} = z'_{n+\Delta N}(d + mD, b + l\Delta w(K)), \quad (2.5)$$

$$\sigma = \sqrt{\frac{1}{(M+1)(L+1)} \sum_{m=-M/2}^{M/2} \sum_{l=-L/2}^{L/2} |Z_{m,l}|^2}, \quad (2.6)$$

$$\sigma' = \sqrt{\frac{1}{(M+1)(L+1)} \sum_{m=-M/2}^{M/2} \sum_{l=-L/2}^{L/2} |Z'_{m+\Delta m, l+\Delta l}|^2}, \quad (2.7)$$

where $*$ denotes the complex conjugate, D is the sampling interval ($19.25 \mu\text{m}$) in the depth direction, Δm and Δl are the radial and longitudinal shifts between ROIs in the n -th and $(n + \Delta N)$ -th frames, respectively, ΔT is the period between two consecutive frames [$\Delta T = 1/(\text{frame rate}) = 5.2 \text{ ms}$], and $\Delta N\Delta T$ is the frame interval for the calculation of the correlation function. In this study, ΔN was set to 10.

The complex correlation function $\gamma(n; \Delta m, \Delta l)$ between the n -th and $(n + \Delta N)$ -th frames is obtained at each of the radial and longitudinal shifts, Δm_n and Δl_n , of the ROI in the $(n + \Delta N)$ -th frame relative to the position of the ROI in the n -th frame. The radial and longitudinal displacements are determined from the radial and longitudinal shifts, $\widehat{\Delta m}_n$ and $\widehat{\Delta l}_n$, which maximize the magnitude of the complex correlation coefficient, $\gamma(n; \Delta m, \Delta l)$. From the estimated radial and longitudinal shifts, $\widehat{\Delta m}_n$ and $\widehat{\Delta l}_n$, the radial and longitudinal average velocities, $\bar{v}_r(n)$ and $\bar{v}_l(n)$, between the n -th and $(n + \Delta N)$ -th frames are respectively given by

$$\bar{v}_r(n) = \frac{c_0 \widehat{\Delta m}_n}{2f_s \Delta N \Delta T}, \quad (2.8)$$

$$\bar{v}_l(n) = \frac{\Delta w(K) \widehat{\Delta l}_n}{\Delta N \Delta T}, \quad (2.9)$$

where c_0 and f_s are the sound speed and sampling frequency, respectively. Then, the radial and longitudinal displacements, $\widehat{x}_r(n)$ and $\widehat{x}_l(n)$, at the n -th frame are estimated as follows:

$$\widehat{x}_r(n+1) = \widehat{x}_r(n) + \bar{v}_r(n)\Delta T, \quad (2.10)$$

$$\widehat{x}_l(n+1) = \widehat{x}_l(n) + \bar{v}_l(n)\Delta T. \quad (2.11)$$

The instantaneous position of the ROI in the $(n + 1)$ -th frame is determined by $\widehat{x}_l(n)$ and $\widehat{x}_r(n)$.

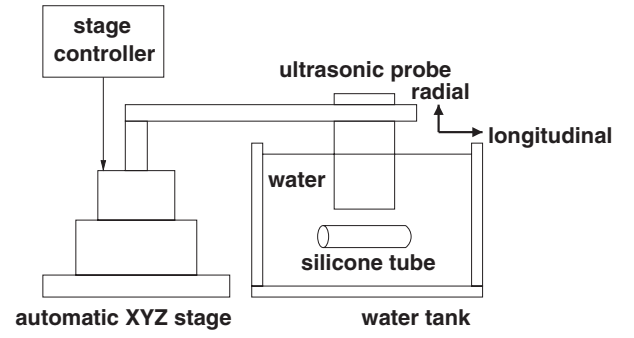


Fig. 1. Experimental system using a silicone tube.

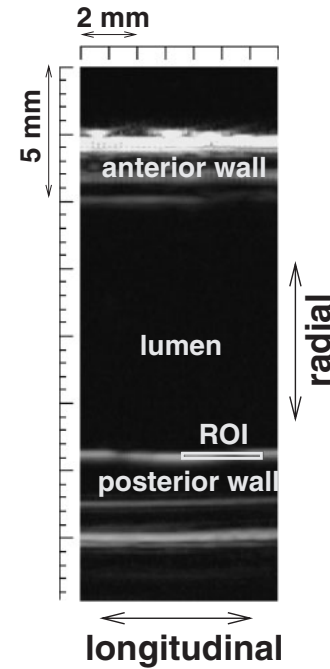


Fig. 2. B-mode image of the silicone rubber tube.

3. Basic Experiments Using a Silicone Tube for Determining the Number of Interpolated Lines

3.1 Displacement estimation

Figure 1 shows the experimental system. In the basic experiment, an ultrasonic probe was moved with a constant speed in the longitudinal and radial directions of a silicone tube using an automatic stage.

Figure 2 shows a B-mode image of the silicone tube. In this experiment, the luminal surface of the silicone rubber was made rough because echoes from a smooth luminal surface are uniform in the longitudinal direction of the tube and there will be no distinct feature to be tracked. The ROI size was set to 2.8 mm (longitudinal) \times 0.2 mm (radial). The radial width was set to 0.2 mm since the size should be smaller than the intima-media thickness.

3.2 Evaluation of random error

Random error was defined as the standard deviation of the estimated velocity. One of sources of random error is the variation in correlation coefficient due to noise. To evaluate the effects of noise, the stage was kept still, and the variance

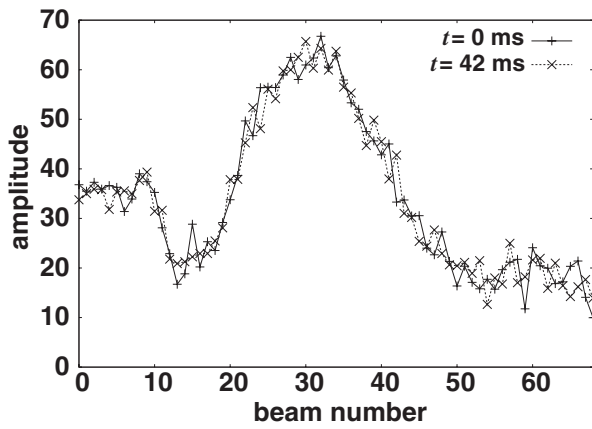


Fig. 3. Amplitudes of RF echoes at $t = 0$ and 42 ms.

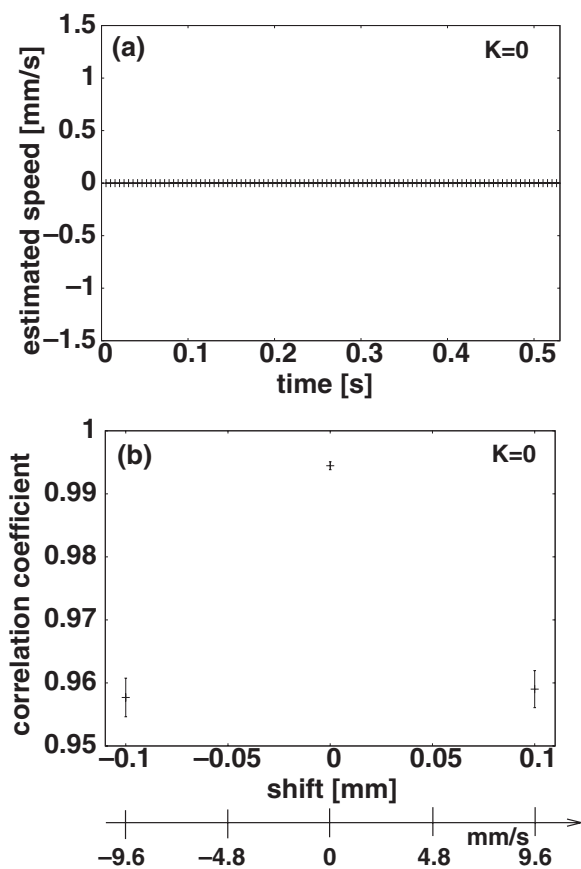


Fig. 4. (a) Estimated speed of silicone tube and (b) the means and standard deviations of the correlation coefficients for $K = 0$. The frame interval $\Delta N\Delta T$ is 0.01 s.

of the correlation coefficient at each shift was evaluated. There should be no variance when there is no noise. Figure 3

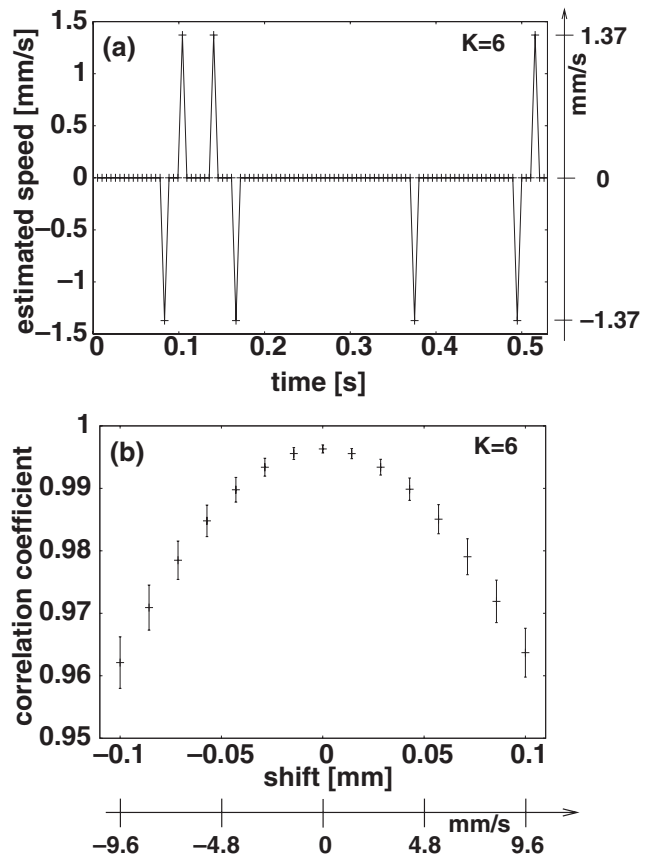


Fig. 5. (a) Estimated speed of silicone tube and (b) the means and standard deviations of the correlation coefficients for $K = 6$. The frame interval $\Delta N\Delta T$ is 0.01 s.

shows the amplitudes of echoes from the silicone tube at $t = 0$ and 42 ms. Although the stage is still, there is a difference between echoes. Figure 4(a) shows the estimated velocity without interpolating RF signals ($K = 0$). In Fig. 4(b), plots and vertical bars show the means and standard deviations of the correlation coefficient, respectively. In Fig. 4, the frame interval $\Delta N\Delta T$ is 10 ms. The mean correlation coefficient at a shift of 0 mm is much larger than those at ± 0.1 mm in comparison with the standard deviation. Therefore, there is no random error in estimated velocity as shown in Fig. 4(a).

However, as shown in Fig. 5, the mean correlation coefficient at a shift of 0 mm is not sufficiently larger than those at ± 0.014 mm when the number K of interpolated lines and frame interval $\Delta N\Delta T$ are 6 and 10 ms, respectively. Therefore, there are random errors in the estimated velocity as shown in Fig. 5(a). The random error e_{random} in the estimated displacement during the period of 2 frames is defined as follows:

$$e_{\text{random}} = \sqrt{\frac{1}{N} \sum_{n=0}^{N-1} \left(\hat{v}_l(n) \Delta N\Delta T - \frac{1}{N} \sum_{n=0}^{N-1} \hat{v}_l(n) \Delta N\Delta T \right)^2}. \quad (3.1)$$

3.3 Evaluation of bias error

Figures 6(a) and 6(b) show the correlation coefficient at each shift Δl_n and the estimated and true (assigned stage speed) longitudinal velocities at each time, respectively. In

Fig. 6, the correlation coefficient reaches its maximum value at a shift corresponding to the true velocity. However, in most cases, the true shift is located between echo lines (including interpolated ones), and the shift that is closest to

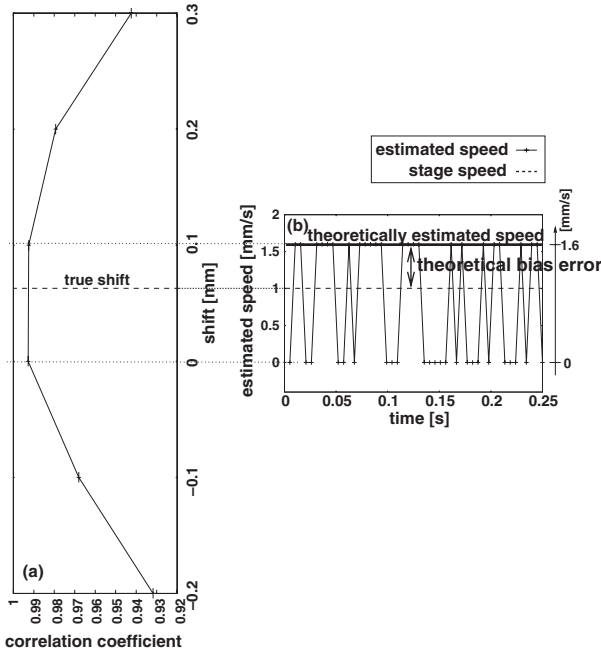


Fig. 6. (a) Correlation coefficient at each ROI shift Δl_n . (b) Estimated and true longitudinal velocities at each time.

the true shift is selected to be the estimate when there is no noise. This shift which is the closest to the true shift is denoted by the theoretically estimated shift (velocity). Thus, the theoretical bias error in the estimated velocity can be defined as the difference between the theoretically estimated velocity and the true one. The maximum value of the theoretical bias error e_{bias} is given by half of the interval $\Delta w(K)$ between interpolated echo lines as follows:

$$e_{\text{bias}} = \frac{\Delta w(K)}{2} = \frac{0.1}{(K + 1) \times 2}. \quad (3.2)$$

Theoretical bias error e_{bias} will be reduced by increasing the number of interpolated lines, K .

3.4 Optimum number of interpolation lines

The optimum number of interpolation lines, K_{opt} , was determined by theoretical bias error e_{bias} and random error e_{random} . Bias error e_{bias} can be theoretically reduced by increasing the number of interpolated lines, K . However, a smaller interval of echo lines (means a larger K) leads to increase in random error e_{random} due to the variance in correlation coefficient. Therefore, the number of interpolation lines K_{opt} , at which random error e_{random} is similar to bias error e_{bias} , is sufficient. Since e_{random} increases with increasing K , the estimation error cannot be reduced by a K larger than K_{opt} .

Figure 7(a) shows the random error e_{random} at each theoretical bias error e_{bias} . Figure 7(b) is an enlarged view of Fig. 7(a). In Figs. 7(a) and 7(b), the theoretical bias error e_{bias} is not significantly reduced at a K that is larger than 8, and e_{bias} is reduced, similar to random error e_{random} at $K = 8$. Therefore, the number K of interpolation lines was determined to be $K = 8$ (beam interval of $11 \mu\text{m}$).

4. Basic Experiments Using Silicone Tube for Detection of Outer Boundary of Wall

Figure 8 shows the experimental system. The difference

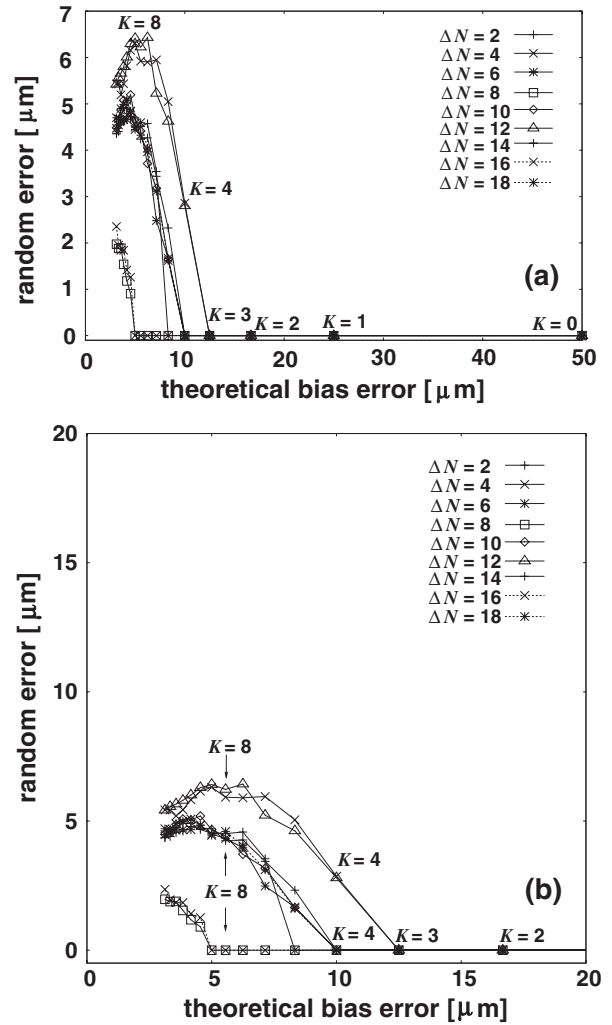


Fig. 7. (a) Random errors e_{random} in the estimated displacements at each theoretical bias error e_{bias} . (b) Enlarged view of (a).

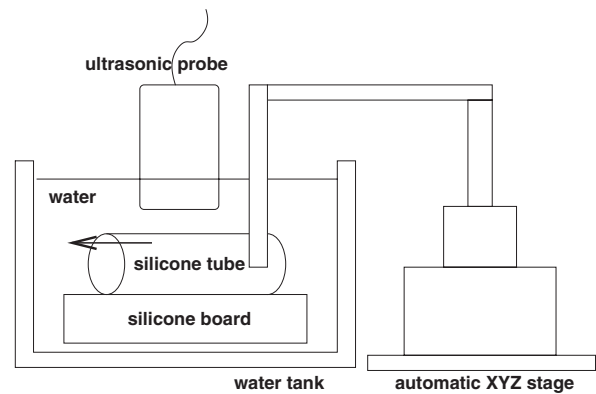


Fig. 8. Experimental system for the boundary detection.

among the longitudinal displacements around the outer boundary of the wall was investigated using a silicone tube on a silicone plate mimicking the external tissue. The stage speed was set to 4 mm/s , and the longitudinal displacement of the silicone tube was estimated. The frame rate was $1/\Delta T = 192 \text{ Hz}$.

Figure 9 shows a B-mode image of the silicone tube on the silicone plate. The longitudinal displacements were estimated at depth positions A, B, C, and D. Figure 10 shows

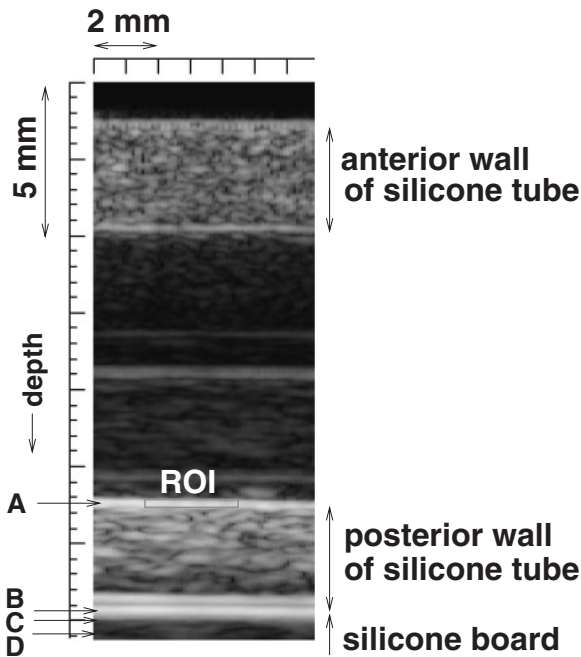


Fig. 9. B-mode image of the silicone tube on the silicone plate.

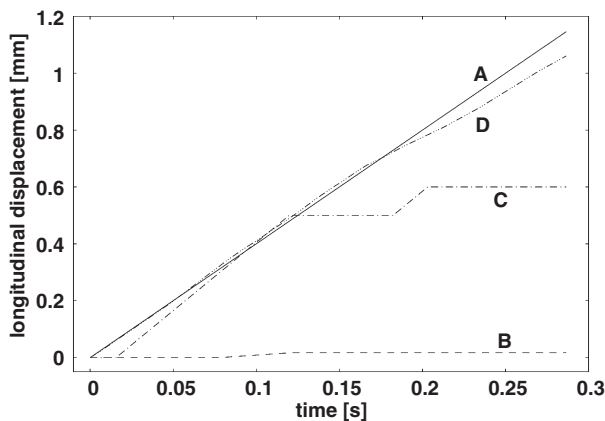


Fig. 10. Longitudinal displacements at depth positions A, B, C, and D at each time.

the estimated longitudinal displacements at each time at depth positions A, B, C, and D. The longitudinal displacements were different depending on the depth.

In Fig. 11, the longitudinal displacements at a time of 0.15 s are shown at each depth position along a line. Figure 11 shows (a) RF echoes from the silicone tube and the silicone board, (b) the longitudinal displacement distribution along the line, and (c) the means and standard deviations of the maximum correlation coefficients from 0 to 0.15 s. In Fig. 11(b), the longitudinal displacement rapidly decreased at a depth position of 3.2 mm. Figure 12 shows the RF echo from the same silicone tube without the silicone plate. In Fig. 12, the thickness of the wall is found to be 3 mm. Therefore, the longitudinal displacement was found to change at the boundary.

5. *In vivo* Measurement

The longitudinal and radial displacements of a carotid artery of a 25-year-old male are estimated using the

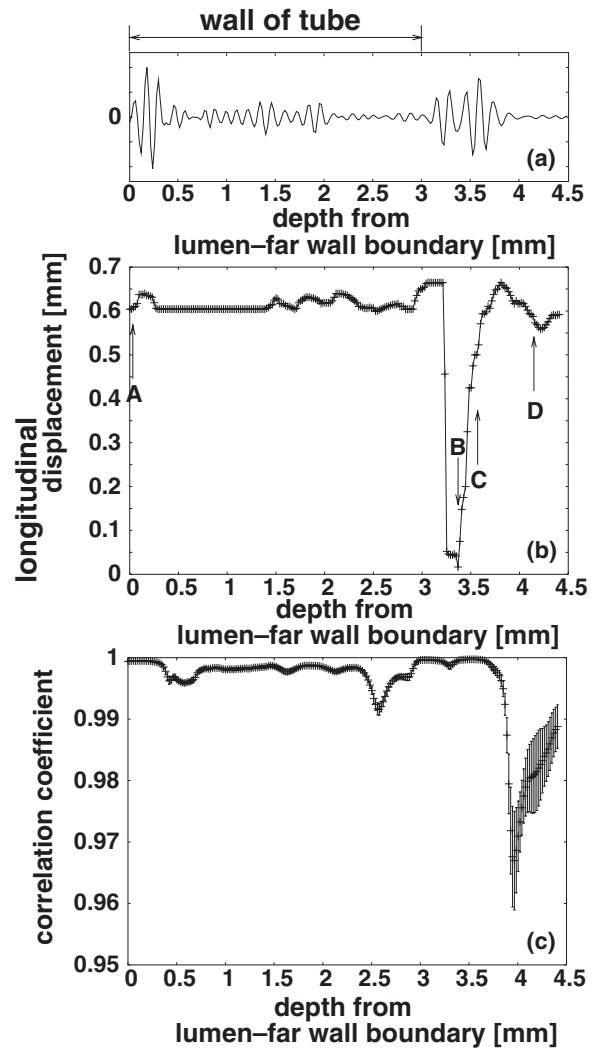


Fig. 11. (a) RF echo from the silicone tube and silicone plate. (b) Longitudinal displacement distribution along the ultrasonic beam. (c) Means and standard deviations of the maximum correlation coefficients averaged during the period from 0 to 0.15 s.

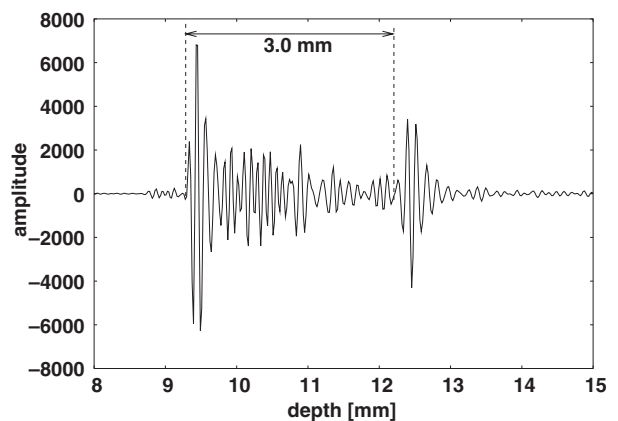


Fig. 12. RF echo from the silicone tube.

determined optimum number of interpolation lines $K_{opt} = 8$ and a frame interval $\Delta N \Delta T = 44$ ms ($\Delta N = 4$, $\Delta T = 1/90$ Hz = 11 ms). Figure 13 shows (a) a B-mode image of the carotid artery, (b) an electrocardiogram, and (c) and (d) estimated longitudinal and radial displacements, respective-

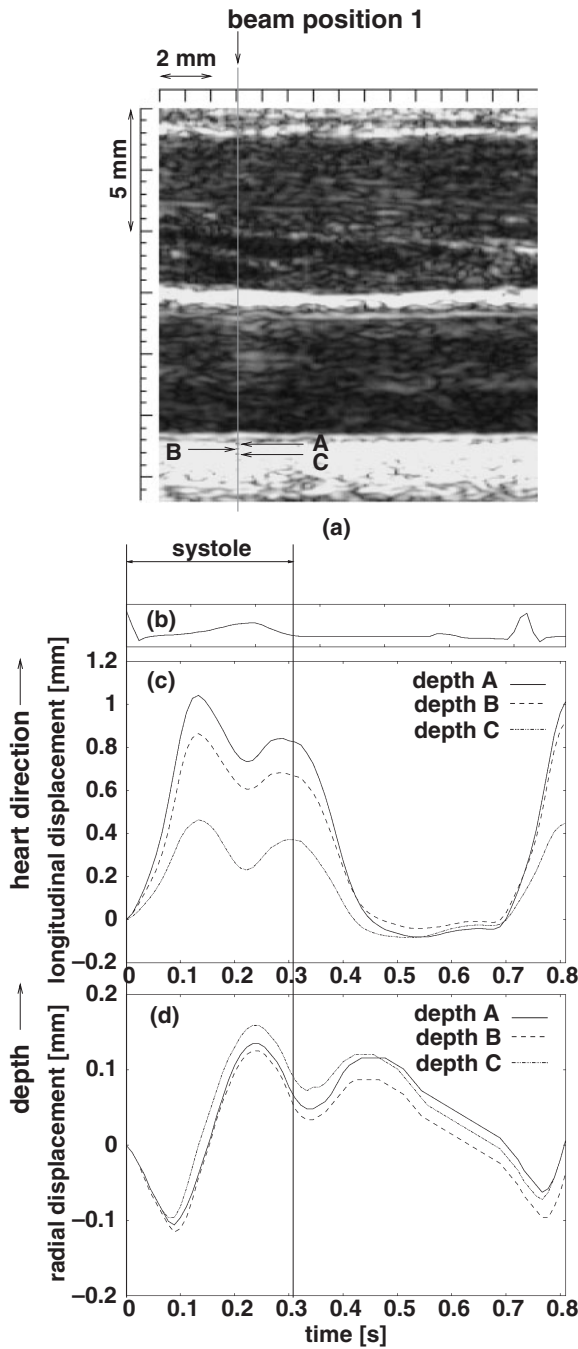


Fig. 13. (a) B-mode image of the carotid artery. (b) Electrocardiogram. (c) Estimated longitudinal and (d) radial displacements of the carotid arterial wall.

ly, of the carotid arterial wall during one cardiac cycle at positions A, B, and C. The waveforms of the longitudinal and radial displacements are similar at each position. However, the amplitudes of the longitudinal displacements are different among the measured positions. The difference in amplitude between depth positions B and C is larger than that between depth positions A and B.

Figure 14 shows (a) RF echo in the range from 0 mm (luminal surface) to 1.3 mm along an ultrasonic beam, (b) the longitudinal displacement at a time $t = 0.13$ s in Fig. 13(c), and (c) the means and standard deviations of the maximum correlation coefficients for the period from 0 to 0.13 s. This time of $t = 0.13$ s was determined by the first

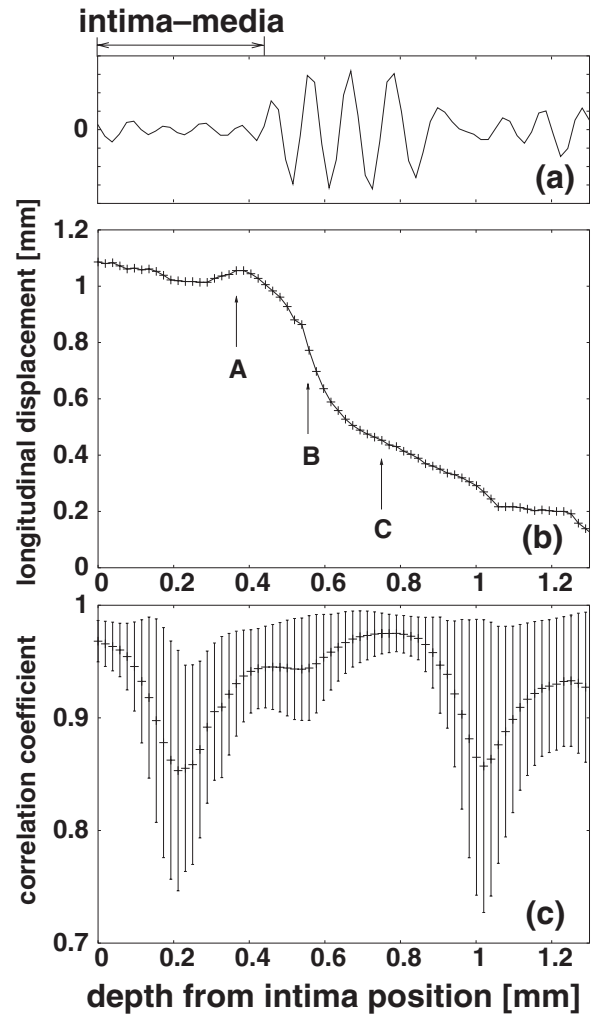


Fig. 14. (a) RF echo from the region from intima (0 mm) to a depth of 1.3 mm. (b) Longitudinal displacement distribution along the ultrasonic beam. (c) Means and standard deviations of the maximum correlation coefficients for the period from 0 to 0.13 s.

peak of the longitudinal displacement shown in Fig. 13(c). The correlation values are sufficiently large at points A, B, and C. However, there are differences in longitudinal displacements among these points.

Figure 15 shows a B-mode image of the carotid artery of the same subject. The longitudinal displacements were estimated at two different ultrasonic beams. Figure 16 shows the longitudinal displacements at beam positions 1 and 2 at the depth A plotted as a function of time.

As shown in Fig. 13, the carotid artery moves toward the heart when the heart ejects blood. The longitudinal displacements decreased between 0.1 and 0.2 s. It is supposed that the carotid artery is pulled by the movement of the base of the heart toward the apex during systole from 0 to 0.1 s. Then, the longitudinal displacement is decreased by the shear stress of blood flow from 0.1 to 0.2 s.

In Fig. 14, the longitudinal displacement decreased rapidly in the region of around 0.6 mm. It is thought that the longitudinal displacement decreased around the outer boundary of the arterial wall, which is similar to the basic experimental results in Fig. 11(b).

The longitudinal displacements at different beam positions were compared to evaluate the stretch of the carotid

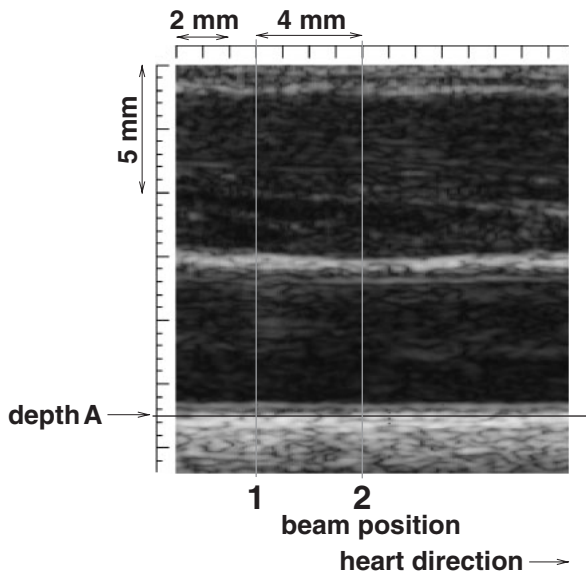


Fig. 15. B-mode image of the carotid artery.

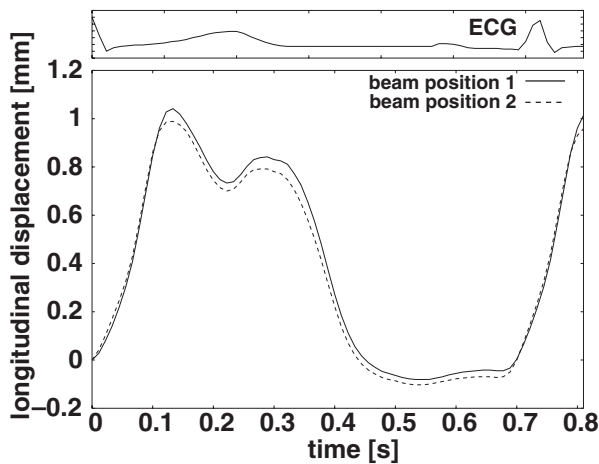


Fig. 16. Longitudinal displacements at beam positions 1 and 2.

arterial wall. Figure 17 shows the longitudinal displacement distributions along the two beams. In this figure, the longitudinal displacements at a time of 0.13 s are shown at each depth position along the corresponding lines.

Although the longitudinal displacements on two beam positions were different in Fig. 16, the longitudinal displacement at beam position 1 is biased from that at beam position 2 as typically shown from 0.4 to 0.7 s, and this difference is considered to be a bias error. Therefore, it is considered that the difference between the longitudinal displacements was small and the carotid arterial wall between two beams was not stretched in the longitudinal direction. However, the rapid decreases in longitudinal displacements around the outer boundary of the arterial wall were found in both beams.

6. Discussion

In this study, the optimum number of interpolation lines, K_{opt} , was investigated by evaluating the variance in correlation coefficient due to noise. Such an investigation is also important for methods in which the correlation peak

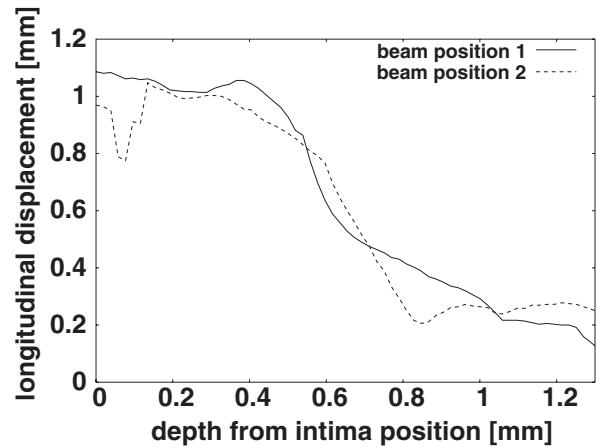


Fig. 17. Longitudinal displacement distributions at beam positions 1 and 2.

is detected by the curve fitting of the correlation function¹⁵⁾ because the variance in correlation coefficient also leads to error in the curve fitting. The estimation accuracies of the proposed method and the curve fitting method should be compared in future work.

In addition, there are parameters whose optimums were not investigated in this study. For example, the optimum frame interval depends on the velocity of an object whereas the frame interval $\Delta N \Delta T$ was set to be constant in this study. The detectable displacement Δx_l between two frames over a line interval is shown using the longitudinal velocity v_l and frame interval $\Delta N \Delta T$ as follows:

$$\Delta x_l = v_l \Delta N \Delta T \geq \Delta w(K). \quad (6.1)$$

Therefore, ΔN should be

$$\Delta N \geq \frac{\Delta w(K)}{v_l \Delta T}. \quad (6.2)$$

However, in *in vivo* measurement, the correlation coefficient is reduced by increasing the frame interval because the echo pattern in a ROI is changed by the arterial wall deformation.¹⁶⁾ Therefore, the frame interval needs to be as short as possible, and ΔN should be $\Delta w(K)/(v_l \Delta T)$.

In this study, a constant frame interval ($\Delta N = 4$ or 10) was employed. However, the following procedure will provide a superior displacement estimate in *in vivo* measurement, although it requires more computation. First, the velocity of longitudinal movement is roughly estimated by a constant frame interval, and the optimum frame interval $\Delta N \Delta T$ is determined at each time using the estimated velocity. Then, the longitudinal displacement is estimated more accurately using the optimum frame interval at each time.

In addition, the optimum ROI size was not investigated. Figure 18 shows the amplitudes of RF echoes from the carotid artery along the longitudinal direction. The longitudinal displacement cannot be detected when there is no variation in echo signals in the ROI. Therefore, the ROI size should be larger than the cycle of the variation of echo signals along the artery. As shown in Fig. 18, the ROI size employed in this paper is sufficiently larger than the cycle of the variation in echo signals. On the other hand, the ROI size should be smaller than the inverse of the spatial frequency of

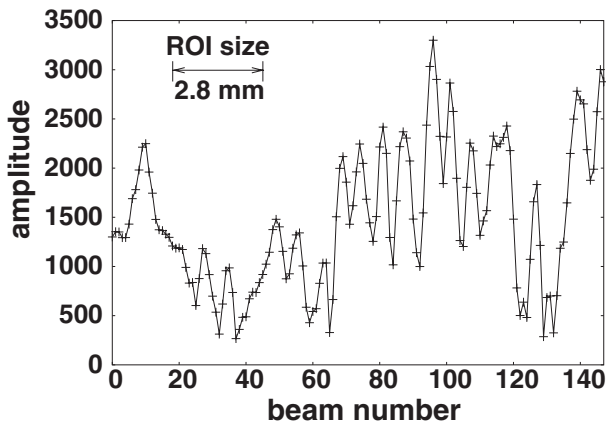


Fig. 18. Amplitude of RF echo along the longitudinal direction in *in vivo* measurement.

the deformation of the arterial wall because the signal pattern in the ROI will be significantly changed by the deformation with a larger ROI. The carotid artery measured in this study showed almost no deformation in its longitudinal direction, and a large ROI was considered not to affect the estimation accuracy so much. However, the carotid arteries of other subjects should be measured to investigate the deformation of the arterial wall in its longitudinal direction. Furthermore, the silicone rubber tube used in the basic experiments of this study shows no deformation. The deformation of the wall may affect the optimization of the number of interpolated echo lines.

As described above, although some remaining problems require further investigation, the proposed method in this paper is useful for a detailed investigation of vessel wall movements.

7. Conclusions

In basic experiments using a silicone tube, the number of interpolation lines for the estimation of the longitudinal displacement was determined by considering bias and random errors. Using the optimum number of interpolation lines, the spatial distribution of longitudinal displacements

along the arterial radial direction was estimated in *in vivo* measurement in the carotid artery. The longitudinal displacement rapidly decreased around the position that is considered to be the outer boundary of the arterial wall, and this result was similar to that in the measurements in a silicone tube on a silicone plate mimicking an artery surrounded by external tissue. These results show that the proposed method has the potential to be used in detecting the outer boundary of adventitia on the basis of the measured displacement distribution.

- 1) H. Hasegawa, H. Kanai, N. Hoshimiya, and Y. Koiwa: *J. Med. Ultrason.* **31** (2004) 81.
- 2) H. Hasegawa, H. Kanai, N. Hoshimiya, N. Chubachi, and Y. Koiwa: *Jpn. J. Appl. Phys.* **37** (1998) 3101.
- 3) H. Kanai, H. Hasegawa, M. Ichiki, F. Tezuka, and Y. Koiwa: *Circulation* **107** (2003) 3018.
- 4) N. Nakagawa, H. Hasegawa, and H. Kanai: *Jpn. J. Appl. Phys.* **43** (2004) 3220.
- 5) J. Tang, H. Hasegawa, and H. Kanai: *Jpn. J. Appl. Phys.* **44** (2005) 4588.
- 6) J. Inagaki, H. Hasegawa, H. Kanai, M. Ichiki, and F. Tezuka: *Jpn. J. Appl. Phys.* **44** (2005) 4593.
- 7) J. Inagaki, H. Hasegawa, H. Kanai, M. Ichiki, and F. Tezuka: *Jpn. J. Appl. Phys.* **45** (2006) 4732.
- 8) M. Persson, Å. R. Ahlgren, A. Eriksson, T. Jansson, H. W. Persson, and K. Lindström: *Proc. IEEE Ultrasonics Symp.*, 2002, p. 1739.
- 9) S. Golemati, A. Sassano, M. J. Lever, A. A. Bharath, S. Dhanjil, and A. N. Nicolaidis: *Ultrasound Med. Biol.* **29** (2003) 387.
- 10) M. Cinthio, Å. R. Ahlgren, T. Jansson, A. Eriksson, H. W. Persson, and K. Lindström: *IEEE Trans. Ultrason. Ferroelectr. Freq. Control* **52** (2005) 1300.
- 11) M. Cinthio, Å. R. Ahlgren, J. Bergkvist, T. Jansson, H. W. Persson, and K. Lindström: *Am. J. Physiol. Heart Circ. Physiol.* **291** (2006) 394.
- 12) J. Bang, T. Dahl, A. Bruinsma, J. H. Kaspersen, T. A. N. Hernes, and H. O. Myhre: *Ultrasound Med. Biol.* **29** (2003) 967.
- 13) J. C. Russ: *The Image Processing Hand Book* (CRC Press, Boca Raton, 1995) 2nd ed.
- 14) J. A. Hossack, T. S. Sumanaweera, S. Napel, and J. S. Ha: *IEEE Trans. Ultrason. Ferroelectr. Freq. Control* **49** (2002) 1029.
- 15) I. Céspedes, Y. Huang, J. Ophir, and S. Spratt: *Ultrason. Imaging* **17** (1995) 142.
- 16) H. Hasegawa, H. Kanai, N. Hoshimiya, and Y. Koiwa: *Jpn. J. Appl. Phys.* **39** (2000) 3257.